Tris-benzo[cd]indole Cyanine Enables the NIR-photosensitized Radical and Thiol-ene Polymerizations at 940 nm

Christine Elian, Benjamin Mourot, Camil Benbouziyane, Jean-Pierre Malval, Sonia Lajnef, Fabienne Peyrot, Florian Massuyeau, Olivier Siri, Denis Jacquemin, Simon Pascal, et al.

Tris-benzo[*cd*]indole Cyanine Enables the NIR-photosensitized Radical and Thiol-ene Polymerizations at 940 nm

Christine Elian,[a]+ Benjamin Mourot,[b]+ Camil Benbouziyane,[b] Jean-Pierre Malval,[c] Sonia Lajnef,[d] Fabienne Peyrot,[d][e] Florian Massuyeau,[f] Olivier Siri,[b] Denis Jacquemin,*[g][h] Simon Pascal,*[b][g] and Davy-Louis Versace*[a]

[a] *Institut de Chimie et des Matériaux Paris-Est, UMR-CNRS 7182-UPEC, 2-8 rue Henri Dunant, 94320 Thiais, France*
E-mail: davy-louis.versace@u-pec.fr

[b] *Centre Interdisciplinaire de Nanoscience de Marseille (CINaM), Aix Marseille Univ, CNRS UMR 7325, Campus de Luminy, Marseille cedex 09 13288, France*
E-mail: simon.pascal@cnrs.fr

[c] *Institut de Science des Matériaux de Mulhouse (IS2M), Université de Haute-Alsace, CNRS UMR 7361, 15, rue Jean Starcky, Mulhouse 68057, France*

[d] *Université Paris Cité, CNRS, Laboratoire de Chimie et Biochimie Pharmacologiques et Toxicologiques, F-75006 Paris, France*

[e] *Sorbonne-Université, Institut National Supérieur du Professorat et de l'Education (INSPE) de l'Académie de Paris, F-75016 Paris, France*

[f] *Nantes Université, CNRS, Institut des Matériaux de Nantes Jean Rouxel, IMN, F-44000 Nantes, France*

[g] *Nantes Université, CNRS, CEISAM, UMR 6230, Nantes, F-44000, France*
E-mail: Denis.Jacquemin@univ-nantes.fr; simon.pascal@cnrs.fr

[h] *Institut Universitaire de France (IUF), Paris F-75005, France*

[+] *These authors contributed equally to this work.*

Supporting information available: https://onlinelibrary.wiley.com/doi/abs/10.1002/anie.202305963. It contains the protocols and characterizations, including ^{1}H, ^{13}C and ^{19}F NMR, HRMS and IR spectra. Additional spectroscopic (electronic absorption, emission, EPR, cyclic voltammetry, photolysis) and theoretical results are also described.

Keywords: Polymethine • Photoinitiator • Photopolymerization • Near-Infrared • Spectroscopy

ABSTRACT

A near-infrared-absorbing heptamethine (**HM**$^{+}$) incorporating three bulky benzo[*cd*]indole heterocycles was designed to efficiently prevent self-aggregation of the dye, which results in a strong enhancement of its photoinitiating reactivity as compared to a parent bis-benzo[*cd*]indole heptamethine (**HMCl**$^{+}$) used as a reference system. In this context, we highlight an efficient free-radical NIR-polymerization up to a 100% acrylates C=C bonds conversion even under air conditions. Such an important initiating performance was obtained by incorporating our NIR-sensitizer into a three-component system leading to its self-regeneration. This original photoredox cycle was thoroughly investigated through the identification of each intermediary species using EPR spectroscopy.

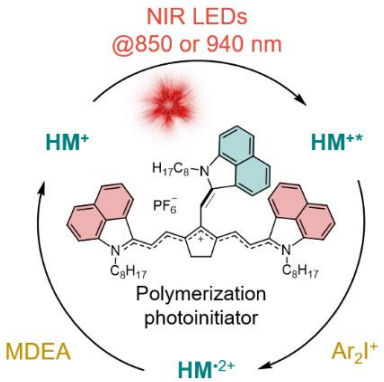

Introduction

Since the emergence of the concept of green chemistry, photopolymerization has established itself as a technique of choice for the synthesis of new valuable materials. This technique has indeed experienced tremendous growth over the last decade, notably through the development of the 3D photo-printing technology in adhesive and coating applications.[1,2] Compared to thermal polymerization, photopolymerization benefits from many striking advantages such as low energy consumption, fast polymerization reactions at room temperature or below, mild experimental conditions without the use of harmful solvents, fewer side reactions, along with spatial and temporal control. From an environmental point of view, the energy consumption and the release of volatile and toxic molecules are highly reduced. UV light irradiation is usually employed to ensure high photopolymerization rates and final photoreactive function conversions. However, such high energy radiation has its drawbacks, *e.g.,* skin and eyes damages, as well as ozone production by wavelengths under 250 nm. To prevent these harmful outcomes, a second generation of photoinitiating systems with absorptions in the visible region have been designed. This trend has been significantly accelerated with the recent progress of light-emitting diode (LED) technology and laser emission sources. The utilization of high-intensity near-infrared (NIR) emission devices and semiconductor lasers also perfectly fits into the framework of the replacement of older techniques based on mercury lamps,[3–6] but requires NIR-absorbing dyes. During the last decades, NIR photosensitizers found applications in different domains, *e.g.*, bio-imaging, photothermal therapy, organic electronics, and non-linear optical applications.[7–14] Surprisingly, few investigations deal with photopolymerization using NIR light sources despite several obvious benefits, as such light: i) is safer than UV light since less energetic radiations are used, ii) has a deeper penetration in biological media,[15] iii) allows the synthesis of thick materials that cannot be addressed with common UV or visible photoinitiating systems due to scattering issues of the resin,[16] and iv) paves the way towards high polymerization rates under low excitation energies in contrast to thermal solutions.[17]

Another key issue for polymerization processes under light irradiation concerns the design of new photoinitiating systems absorbing at much longer wavelengths, especially in the NIR region, to prevent side reactions such as the self-initiation of monomers and the degradation of already-formed oligomers. Even though an increasing number of visible absorbing (400–750 nm) photoinitiating systems became available during the last decade,[18–22] literature reporting NIR photosensitizers for polymerization under irradiation above 800 nm is scarce and remains a *hot topic* because the low photon energy strongly decreases the energy available to initiate the chemical process. Notably, Boyer and co-workers have demonstrated that radical addition fragmentation transfer (RAFT) polymerization could be initiated with phthalocyanine derivatives and bacteriochlorophyll by far-red to NIR sensitization.[18–22] Recently, a diaminium hexafluoroantimonate sensitizer absorbing beyond 1000 nm was used in a three-component initiating system to initiate the free-radical polymerization (FRP) of acrylate monomers introducing three to four reactive functions.[23] Also, Lalevée and coworkers reported the photopolymerization of methacrylate-based monomers upon laser diode (LD) at 785 nm and 940 nm, with four-component photoinitiating systems based on iodonium salt, phosphine, a thermal initiator and various squarylium polymethine dyes; the latter showing however a low absorption in the irradiation range.[24]

The craze surrounding polymethine cyanines has been renewed recently due to the straightforward access to NIR-absorbing candidates within this family,[25,26] used notably for applications as chemosensors,[27] for solar cells[28] and nonlinear optics,[14,29] but also as photosensitizers for polymerization process.[30] These sensitizers are characterized by high molar extinction coefficients from the red to the NIR region and can be conveniently engineered to tune their optical features or their photochemical stability under light irradiation.[3,25,31–33] In 2015, the reactivity of new iodonium salts as radical initiators was studied for the first time by photo-differential scanning calorimetry (photo-DSC) using a zwitterionic heptamethine-barbiturate dye as photosensitizer. The radical photopolymerization of multifunctional acrylic monomers was successfully demonstrated with the zwitterionic cyanine dye/iodonium salt NIR photoinitiating system under LED@780 nm excitation.[34] Next, Strehmel and co-workers reported the electron transfer reaction between iodonium salts and the excited states of cyanine derivatives absorbing in the 750–850 nm region, thus highlighting the formation of radical and photoacid initiating species.[35,36] Similar results were obtained in 2017 according to a photosensitized mechanism between a polymethine derivative as sensitizer and different substituted diaryliodonium salts bearing weak coordinating anions as co-initiator under LED@790 nm.[37] Interestingly, this opened new opportunities for the synthesis of thicker coatings by NIR LED irradiation.[38] Polymethine-based

compounds have been then used to sensitize ATRP when combined with ppm of a Cu(II)/*tris*(2-pyridylmethyl)amine catalyst and α-bromophenylacetate considered as the alkyl halide initiator.[39] The first report of cationic photopolymerization under NIR LED device dates from 2019.[3] Strehmel and co-workers enlarged the possibilities of NIR photopolymerization by combining heptamethine derivatives and iodonium salts for the radical and cationic photopolymerizations of tripropylene glycol diacrylate and epoxides derived from bisphenol-A-diglycidylether, respectively, under high-power LED emitting at 805 nm. Recently, the selection of appropriate fluorinated phosphate counterions on iodonium salts structures have gain growing considerations to drive their reactivity when coupled with cationic heptamethine derivatives. Cationic photopolymerizations of epoxides, vinyl ether, and oxetane were then demonstrated, and the synthesis of interpenetrating polymer networks using multiacrylate monomers and epoxides successfully occurred under NIR-LED@805 or 870 nm.[40,41]

The lack of EPR investigations in polymethine-based NIR photosensitive systems prompted us to understand the photopolymerization mechanisms related to the photosensitization of a iodonium salt (*i.e.*, *bis*(4-methyl phenyl)iodonium hexafluorophosphate salt, Iod) by an original cyanine sensitizer (tris-benzo[*cd*]indole-based heptamethine, **HM$^+$**) in the presence of reducing agent (*N*-methyl diethanol amine, MDEA) or H-donor compound (trimethylolpropane *tris*(3-mercaptopropionate, TT) by EPR spin-trapping technique. The strong absorbance of **HM$^+$** in the NIR region allows working at very low energy (940 nm) and its large central substituent prevents the aggregation of the dye in solution. The originality of this work relies on the capability of the novel three-component initiating system containing MDEA to successfully accelerate free-radical polymerization at LED@850 and 940 nm, and also to induce thiol-ene reaction process under air with tremendous final vinyl conversions of triethylene glycol divinyl ether (DVE), which have, to the best of our knowledge, never been reported before. This process is of great importance to develop thick materials upon NIR irradiation under air. In the first part of this investigation, the synthesis of a new heptamethine NIR-sensitizer is presented, followed by the evaluation of its light absorption and electrochemical properties. In a second part, the photochemical reactivities of **HM$^+$**/Iod/MDEA and **HM$^+$**/Iod/TT photoinitiating systems toward the free-radical photopolymerization of a multifunctional acrylate monomer (trimethylolpropane triacrylate, TMPTA) and the thiol-ene reaction process, respectively, are evaluated in detail by RT-FTIR and EPR spin trapping experiments.

Results and discussion

The synthesis of benzo[*cd*]indole-based heptamethine cations was carried out by mixing the activated salt **1** and at least two equivalents of the tetrafluoroborate salt **2** in acetic anhydride and in the presence of sodium acetate (Scheme 1). While performing the Knoevenagel condensation at room temperature provided the well-known heptamethine **HMCl$^+$** with moderate yield, increasing the reaction temperature to 80 °C led to the formation of **HM$^+$**, presenting a third benzo[*cd*]indole moiety substituted in the central position of the polymethine bridge. To the best of our knowledge, such substitution pattern was not previously observed, which is rather surprising since analogues of **HMCl$^+$** have been punctually reported in the literature *via* condensation reactions carried out up to 60 °C and could have afforded similar reactivity.[42–44] The structure of **HM$^+$** was confirmed by high-resolution mass spectrometry, showing a molecular peak at *m/z* 924.6190 Da [M$^+$]. ^{1}H NMR spectroscopy revealed two sets of doublets with coupling constants ^3J *ca*. 13–14 Hz, which are characteristic of the hydrogen atoms borne by the heptamethine bridge being in *trans* configuration (see the SI for details).

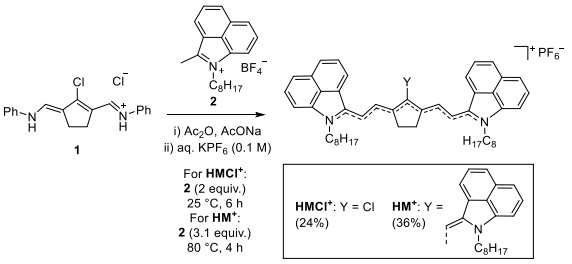

Scheme 1. Synthesis of heptamethines **HMCl$^+$** and **HM$^+$**.

The visible-NIR absorption properties of the two heptamethines depicted in Figure 1 were recorded in CH_2Cl_2 and show intense absorption bands in the 800–1100 nm spectral range, with comparable maxima centered at 1057 nm (ε^{1057} = 175000 M^{-1} cm^{-1}) and 1050 nm (ε^{1050} = 215000 M^{-1} cm^{-1}) for **HMCl$^+$** and **HM$^+$**, respectively. The absorption of the dyes was screened at different concentrations in dichloromethane solution, showing no evidence of aggregation between 10^{-4}–10^{-7} M in this solvent (Figure S27). In less polar ethyl acetate,[45] **HM$^+$** is remarkably more soluble and inert compared to **HMCl$^+$**, which tends to aggregate above 10^{-5} M, and is converted to a red-absorbing species below 10^{-6} M (Figure S28). Moreover, the comparison of the absorption of **HMCl$^+$** in different solvents reveals that it decomposes in DMSO and that the molar extinction coefficients are drastically lowered in ethyl acetate and MeOH (ε^{1053} = 58000 M^{-1} cm^{-1} and ε^{1050} = 76000 M^{-1} cm^{-1}, respectively), accompanied with a

broadening of the absorption profiles compared to dichloromethane (Figure S29). In contrast, **HM**$^+$ maintains strong extinction coefficients in these solvents (ε between 1–2×10^5 M^{-1} cm^{-1}). On the one hand, the higher stability of **HM**$^+$ may be related to the absence of reactive central chlorine atom, but also to the steric protection brought by the large hydrophobic central substituent, preventing the photooxidative cleavage of the polymethine bridge.[46] On the other hand, the solubility improvement going from **HMCl**$^+$ to **HM**$^+$ is attributed to the bulky benzo[*cd*]indole substituted at the *meso* position that prevents aggregation of the dye by reducing the possible intermolecular interactions, as previously reported for benzoindole-based heptamethines introducing a bulky Pd(PPh$_3$)$_2$Cl at the same position.[47] To further illustrate the effect of the central substituent on aggregation, we recorded the absorption of thin films of **HMCl**$^+$ and **HM**$^+$ prepared by spin-coating (see SI for details). The absorption of **HMCl**$^+$ thin film presents a particularly broad profile with a new intense band appearing at *ca*. 800 nm that is presumably due to aggregates (Figure S30). In contrast, the thin film absorption of **HM**$^+$ still exhibits the classical "cyanine" absorption profile while being however broadened and redshifted, with a maximum *ca*. 1200 nm and a shoulder at 950 nm.

HM$^+$ exhibits a good overlap with the emission spectra of 850 and 940 nm LEDs used here, with ε^{850} = 30400 M^{-1} cm^{-1} and ε^{940} = 67500 M^{-1} cm^{-1}, compared to the **HMCl**$^+$ reference (ε^{850} = 11100 M^{-1} cm^{-1} and ε^{940} = 40700 M^{-1} cm^{-1}). When dissolved in solvents of various polarities, the absorption of the tri-substituted heptamethine **HM**$^+$ does not reveal noticeable solvatochromic effect, with maxima varying in the 1034–1061 nm range, *i.e.*, $\Delta\overline{\nu}$ = 246 cm^{-1} (Figure S29). Such behavior indicates an ideal polymethine "cyanine" state, involving a symmetrical delocalization of the cationic charge over a non-alternating polymethine chain (trifling bond length alternation), despite the presence of a strong heterocyclic donor substituted in central position. The lack of absorption band shift when comparing **HM**$^+$ and **HMCl**$^+$ suggests that the central substituent is weakly conjugated to the heptamethine bridge, as confirmed by theoretical calculations (*vide infra*).[31] Interestingly, both heptamethines are emissive in the NIR region, showing fluorescence maxima centered at 1100 nm and 1096 nm for **HMCl**$^+$ and **HM**$^+$, respectively (Figure S31). Their fluorescence quantum yields were determined lower than 1% (Table S1, Figure S32), which is expected for NIR heptamethines, as a consequence of the energy gap law.[48]

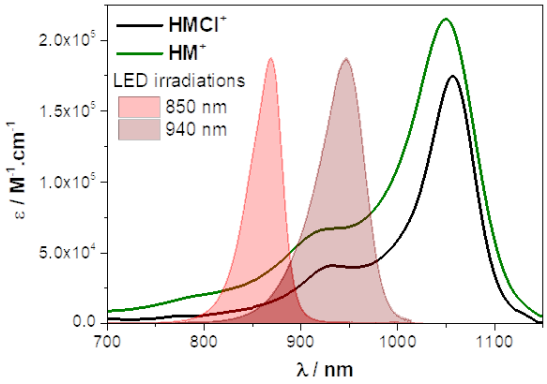

Figure 1. Electronic absorption spectra of **HMCl**$^+$ (black) and **HM**$^+$ (green) in CH_2Cl_2 solutions, superimposed with the emission spectra of the LEDs.

To obtain some insights into the nature of the electronic states of **HM**$^+$ (and **HMCl**$^+$), we used time-dependent DFT (see the SI for details). In **HM**$^+$, the central benzo[*cd*]indole group is significantly twisted (central dihedral angle of *ca*. 50°), and its octyl chain shows weak interactions with one of its counterparts of the main cyanine (Figure S36). The vertical transition energies given by theory are 822 and 825 nm for **HM**$^+$ and **HMCl**$^+$, respectively. These values are blueshifted by 0.33 eV as compared to the experimental λ_{max}, an effect due to the neglect of vibronic couplings and the inherent limitations of TD-DFT for cyanines.[49] More interesting is the electron density difference plot displayed in Figure 2: it shows that the lowest excited state is delocalized on the main π-conjugated path only, with no significant contribution from the central benzo[*cd*]indole moiety nor side naphthyl rings. This explains why both **HM**$^+$ and **HMCl**$^+$ display highly similar optical signatures (Figure 1). One also recognizes the typical cyanine topology with alternation of significant atom-centered gain/loss of density on even/odd nuclei of the cyanine pathway (Figure 2).[31,49]

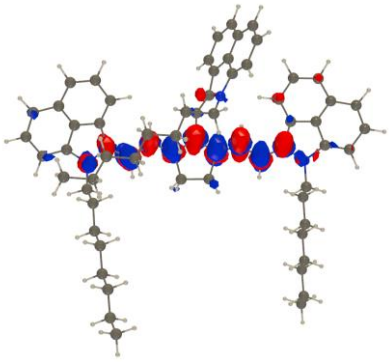

Figure 2. Electronic density difference plot for **HM**$^+$, with in blue (red) the zones corresponding to loss (gain) of electronic density upon photoexcitation (contour 0.001).

As the strong NIR absorption properties of **HM**$^+$ let us foresee its use as a photoinitiator for the free-radical polymerization of acrylates, the dye was first combined with a reducing agent (MDEA), an oxidizing agent (Iod) and a trimethylpropane triacrylate functional monomer (TMPTA). The photoinitiating abilities of the two-component (*i.e.*, **HM**$^+$/MDEA and **HM**$^+$/Iod) and the three-component systems (**HM**$^+$/Iod/MDEA) were investigated upon LEDs@850 and 940 nm irradiation. The corresponding kinetic profiles obtained by RT-FTIR with the three photoinitiating systems are shown in Figure 3 and the final acrylate bond conversion after 800 s of irradiation are listed in Table 1.

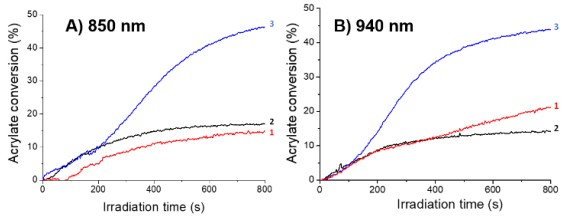

Figure 3. Kinetic profiles of the acrylate function of the NIR-photosensitized TMPTA/**HM**$^+$/MDEA (curve 1), TMPTA/**HM**$^+$/Iod (curve 2) and TMPTA/**HM**$^+$/MDEA/Iod (curve 3) formulations under LED irradiation A) @850 nm and B) @940 nm in laminate. Intensity of LED irradiation = 1 W.cm^{-2}. [Iod] = 3.8 x 10^{-2} mmol.g^{-1} [MDEA] = 4.8 x 10^{-1} mmol.g^{-1} and [**HM**$^+$] = 6 x 10^{-3} mmol.g^{-1}.

Table 1. Acrylate bond conversion (%) determined by IR for the free-radical polymerization of the NIR-photosensitized TMPTA/**HM**$^+$/Iod, TMPTA/**HM**$^+$/MDEA, TMPTA/**HM**$^+$/Iod/MDEA and TMPTA/**HMCl**$^+$/Iod/MDEA formulations in laminate upon LEDs@850 nm and 940 nm irradiation for 800 s. Intensity of the LED irradiation = 1 W.cm^{-2}.

Formulation	Acrylate conversion (%)	
	850 nm	940 nm
TMPTA/**HM**$^+$/Iod	16	15
TMPTA/**HM**$^+$/MDEA	13	20
TMPTA/**HM**$^+$/Iod/MDEA	47	45
TMPTA/**HMCl**$^+$/Iod/MDEA	np[a]	np[a]

[a] np = no polymerization.

First, the addition of only Iod or MDEA to the NIR dye leads to low acrylate conversions, *ca*. 15% after exposure. The photoinitiating abilities of **HM**$^+$/Iod and **HM**$^+$/MDEA are due to the formation of methylphenyl and α-aminoalkyl radicals, respectively, as indicated by the EPR-spin trapping experiments with N-*tert*-butyl-α-phenylnitrone (PBN). In spin trapping experiments, the hyperfine splitting pattern and the values of the hyperfine coupling constants of the EPR spectrum of the spin adduct are characteristic of the type of free radical that is trapped.[50] Indeed, Figure 4 shows for the first time the experimental and simulated EPR spectra of **HM**$^+$/Iod/PBN and **HM**$^+$/MDEA/PBN after LED@850 nm irradiation. The methylphenyl and α-aminoalkyl spin-adducts are evidenced by the respective spin-Hamiltonian parameters a_N = 1.46 mT, a_H = 0.23 mT; g = 2.0061 and a_N = 1.48 mT, a_H = 0.27 mT; g = 2.0058. The methylphenyl radical PBN adduct has a smaller hydrogen coupling constant (a_H = 0.23 mT) than the α-aminoalkyl radical PBN adduct (a_H = 0.27 mT) so they can easily be distinguished (see Figures S37 and S38). The large EPR signal marked by a * in Figure 4 is likely due to the formation of a long-lived carbon-centered radical species (g = 2.0027) on the **HM**$^+$ backbone, as it is observed in the presence of **HM**$^+$ alone. Interestingly, the low EPR ST intensity of the PBN adduct signals may indicate that α-aminoalkyl radicals are present in a low concentration within the solution (Figure 4B). The addition of MDEA to (**HM**$^+$/Iod) photoinitiating system leads to a tremendous increase of EPR ST signal of the α-aminoalkyl radicals (Figure 4D) in comparison with that observed for **HM**$^+$/MDEA photoinitiating system alone (Figure 4B). Going from figure 4B to 4D, the intensity of the EPR spectrum of the corresponding α-aminoalkyl radicals PBN adduct is dramatically increased by a factor of 400. Figure S38 in the supporting information separates the two components observed in the spectrum of the **HM**$^+$/MDEA system, highlighting the component due to α-aminoalkyl radicals in Figure 4B (also, Figure S37 concerns the **HM**$^+$/Iod photoinitiating system). This is a strong evidence corroborating that the radical formation rate in the three-component system is much higher than that observed with **HM**$^+$/MDEA alone, supporting a fast cycling mechanism of the photoinitiating system in the former case (Scheme 2). As a consequence, the subsequent combination of Iod and MDEA to **HM**$^+$ leads to a tremendous increase of the final acrylate conversions whatever the LEDs used (see Figure 3 and Table 1). In comparison, it should be noticed that the inefficient polymerization capability of the **HMCl**$^+$ system is most probably due to its aggregation (*vide supra*). The strong π-π stacking interactions between **HMCl**$^+$ likely yield H-aggregation — the major phenomenon responsible for emission quenching of π-conjugate dye aggregates — which decreases energy transfer from the cyanine to the acceptor molecule. Thermodynamic considerations may also explain the reactivity of the different cyanine based photoinitiating systems. The Rehm Weller equation is used to predict if an electron-transfer reaction at the singlet (or triplet) excited state is thermodynamically possible between **HM**$^+$ and the co-initiators *(i.e.* the electron acceptor, Iod, or the electron donor molecule, MDEA). Importantly, the calculations of the electron-transfer Gibbs energy ΔG

calculated from the Rehm-Weller equation (equation S1, see SI) indicate that the electron transfer reaction at singlet excited state from **HM^{+}*** to Iod ($\Delta G_{HM^{+}*}^{Iod}$ ~ 0.07 eV) is thermodynamically more favorable than that from MDEA to **HM^{+}*** ($\Delta G_{MDEA}^{HM^{+}*}$ = 0.21 eV > 0). These results perfectly fit with electron-transfer reactions between **HM^{+}*** and both co-initiators, which are due to the low oxidation and reduction potentials of **HM^{+}** (E_{ox} = +0.54 V and E_{red} = -0.36 V *vs* SCE, Figure S39). Therefore, methyl phenyl radicals should be more easily produced in a first step than α-aminoalkyl radical. The non-favorable energy transfer reaction between **HMCl^{+}*** (E_{ox} = +0.60 V) and Iod as $\Delta G_{HMCl^{+}*}^{Iod}$ ~ 0.13 eV also confirmed the low photoreactivity of the **HMCl^{+}**-based systems and the low TMPTA acrylate conversions under light irradiation.

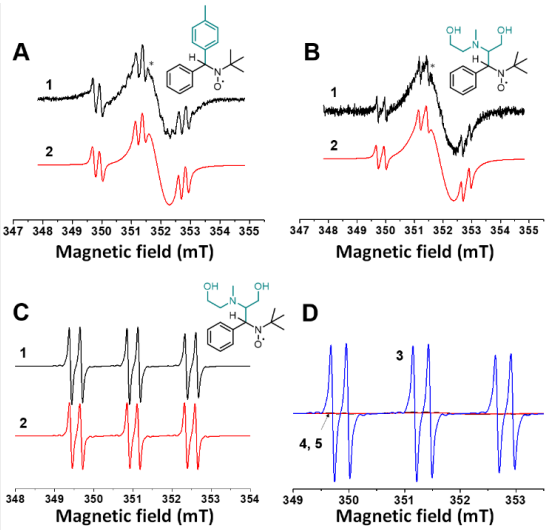

Figure 4. Experimental (1) and simulated (2) EPR spectra obtained during 210 s after exposure (LED@850 nm) of A) **HM^{+}**/Iod/PBN, B) **HM^{+}**/MDEA/PBN and C) **HM^{+}**/Iod/MDEA/PBN systems. D) Comparison of the EPR signals of the **HM^{+}**/Iod/MDEA/PBN (3), **HM^{+}**/Iod/PBN (4), **HM^{+}**/MDEA/PBN (5) and formulations after LED@850 nm irradiation. Reactions occur in CH_2Cl_2 and under argon. Initial concentrations: [**HM^{+}**] = 30 mM; [Iod] = 30 mM; [MDEA] = 420 mM; [PBN] = 0.08 M). EPR spectrometer settings: microwave frequency, ~9.86 GHz; microwave power, 10 mW; center field, ~350 mT; sweep width, 7 mT; gain, 60 dB; modulation amplitude, 0.05 mT; sweep time, ~42 s; time constant, 10.24 ms; and number of scans, 5. The inset shows the structure of the PBN-adduct assigned from the simulated EPR spectrum. * is likely due to the formation of a long-lived carbon-centered radical species on **HM^{+}** backbone.

The proposed mechanism for the photochemical reactivity of the NIR dye in the three-component photoinitiating system is described as follows (Scheme 2): after the NIR light activation, the expected photoelectron transfer reaction from **HM^{+}** to Iod generates the oxidized species **HM$^{\bullet 2+}$** and methylphenyl radicals. At this stage, the generated methylphenyl radicals can abstract a hydrogen atom from MDEA to produce α-aminoalkyl radicals. Subsequently, **HM$^{\bullet 2+}$** is reduced by MDEA thus leading to the formation of α-aminoalkyl radicals and the regeneration of **HM^{+}**.

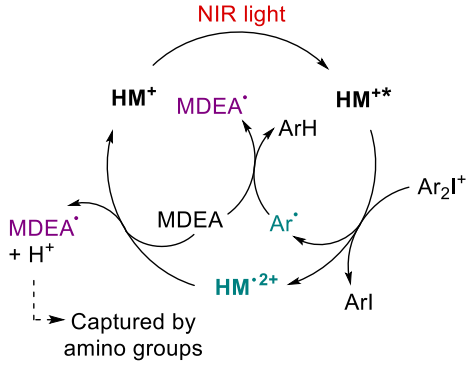

Scheme 2. Proposed mechanism for the irradiation of the three-component (**HM^{+}**/Iod/MDEA) photoinitiating system (Ar = PhMe).

To highlight the intermediary role of **HM$^{\bullet 2+}$** in the photoredox cycle, spectroelectrochemical analysis of **HM^{+}** upon its electrochemical oxidation were performed in acetonitrile. With this respect, it is possible to observe the generation of **HM$^{\bullet 2+}$** through the growth of its spectroelectrochemical spectrum and compare the time-dependent production of this oxidized species in the presence or the absence of MDEA. Indeed, the amine can be initially introduced to promote a subsequent reduction of **HM$^{\bullet 2+}$** once electrogenerated and leads thereby to the regeneration of **HM^{+}**. Note that the applied oxidation potential was maintained at a value of 0.65 V *vs.* SCE in order to exclude the concomitant oxidation of MDEA (E_{ox} = 1 V *vs.* SCE) and further side reactions with the related oxidized species. As shown in Figure 5A, the oxidation of **HM^{+}** clearly leads to a significant decrease of its NIR absorption band with the concomitant appearance of new bands in the 350-600 nm with two maxima located at 390 nm and 515 nm. The growth of this new absorption spectrum should be ascribed to the formation of **HM$^{\bullet 2+}$**. As displayed in Figure S40, a first-order kinetics reaction can be derived by correlating the absorbance change at 920 nm (consumption of **HM^{+}**) with that monitored at 515 nm (production of **HM$^{\bullet 2+}$**). This correlation reasonably agrees with a one electron oxidation process of the NIR dyes. Interestingly, the absorption spectrum of **HM$^{\bullet 2+}$** is not observed any more in presence of 5 equiv. of MDEA (see Figure 5B) and the absorption spectrum of **HM^{+}** remains globally invariant upon applying the oxidation potential. This effect clearly corroborates the role of the amine which is used as a sacrificial reactant promoting a very fast reduction of **HM$^{\bullet 2+}$** with the

regeneration of the NIR dye. Also, the absorption spectra of the three-component system do not show any change after irradiation with LEDs@850 and 940 nm, providing evidence of the regeneration of the heptamethine photosensitizer, along with its good photostability (Figure S41).

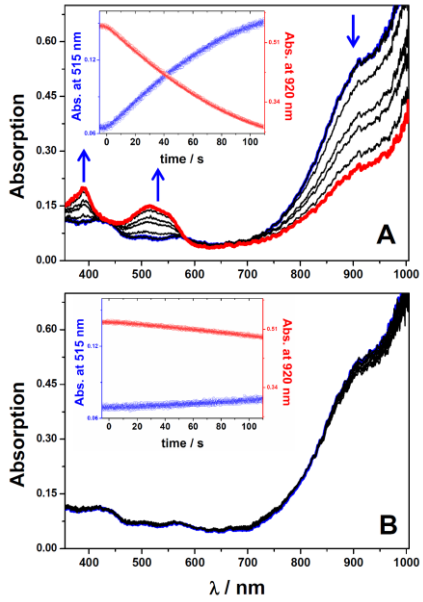

Figure 5. Time-dependent changes of the absorption spectrum of **HM**$^+$ upon its oxidation reaction in acetonitrile without MDEA (A) and with 5 equiv. of MDEA (B). Applied potential: 0.65 V vs. SCE; [**HM**$^+$] = 0.13 mM; [(nBu)$_4$NPF$_6$] = 0.1 M.

It is well known from literature that MDEA is involved in an electron transfer reaction *via* a single electron oxidation of the amine. This process involves a single electron transfer (SET) from the amine to the excited state of the photosensitizer, leading to a MDEA radical cation. The second step consists in a facile deprotonation of the MDEA radical cation, leading to the formation of a photoacid H^+ and the α-aminoalkyl radical.[51] However, a slight release of photoacids H^+ is observed under light irradiation of the (**HM**$^+$/Iod/MDEA/bromophenol sodium salt) system according to the well-known bromophenol test[52] that is used to qualitatively observe the formation of acid (Figure S42). The weak concentration of photoacids captured by bromophenol suggests that the photoproducts comprising amino groups are protonated by H^+, thus drastically reducing the available acid needed to protonate bromophenol, as previously shown by Strehmel and co-workers.[53]

In a nutshell, these experiments reveal a self-sustained process leading to the regeneration of **HM**$^+$ and the increase of the acrylate final conversions. EPR spin-trapping investigations have highlighted the formation of radical species (methylphenyl and α-aminoalkyl radicals) which have been clearly identified when the sensitizer **HM**$^+$ is combined with oxidizing and reducing agents upon NIR irradiation. Besides, the methylphenyl radicals are the cornerstone of the next section dealing with thiol-ene reaction process, notably allowing the reactions to occur under air.

In light with these results, DVE was then used as model to study the reactivity of the NIR-sensitized thiol-ene photopolymerization. The kinetic profiles of the DVE/TT/**HM**$^+$/Iod formulation upon LEDs@850 and 940 nm irradiation, under air and in laminate, are compared with those of the reference DVE/TT/**HMCl**$^+$/Iod formulation in Figure 6, whereas Table 2 summarizes the vinyl and the thiol final bond conversions of both systems after 800 s of irradiation under air and in laminate. The kinetic profiles clearly demonstrate the fast reactivity of the **HM**$^+$/Iod photoinitiating system in comparison with the reference one (**HMCl**$^+$/Iod). Moreover, the final vinyl and thiol conversions of DVE and TT, respectively, are two or three times higher in the presence of **HM**$^+$/Iod photoinitiating system compared to the reference one **HMCl**$^+$/Iod (Figure 7).

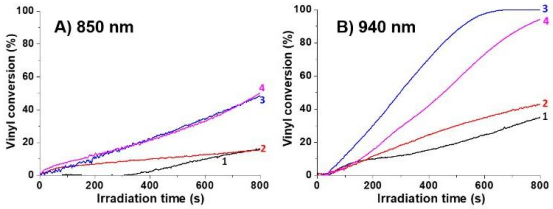

Figure 6. Kinetic profiles of the vinyl function in the blend mixture DVE/TT (50/50 wt%) with **HMCl**$^+$/Iod (curves 2 and 1) or **HM**$^+$/Iod (curves 4 and 3) systems under A) 850 nm and B) 940 nm LED irradiation. Curves 1 and 3: in laminate and curves 2 and 4: under air. Intensity of light = 1 W.cm^{-2}. [Iod] = 3.8 x 10^{-2} mmol.g^{-1} and [**HM**$^+$]=[**HMCl**$^+$] = 6 x 10^{-3} mmol.g^{-1}.

Table 2. Vinyl and thiol bond conversion (%) determined by IR for the thiol-ene reaction process of the NIR-photosensitized DVE/TT/**HM**$^+$/Iod formulation, DVE/TT/**HMCl**$^+$/Iod system (reference), DVE/**HM**$^+$/Iod, DVE/**HM**$^+$ and DVE/Iod formulations under air and in laminate upon LEDs@850 nm and 940 nm irradiation for 800 s.

Formulation	850 nm				940 nm			
	Air		Laminate		Air		Laminate	
	vinyl	thiol	vinyl	thiol	vinyl	thiol	vinyl	thiol
DVE/TT/**HM**$^+$/Iod	46	37	50	40	100	60	95	65
DVE/TT/**HMCl**$^+$/Iod	16	18	15	13	35	27	42	40
DVE/**HM**$^+$/Iod	np[a]	-	np[a]	-	np[a]	-	np[a]	-
DVE/TT	np[a]	np[a]	np[a]	np[a]	np[a]	np[a]	np[a]	np[a]
DVE/Iod	np[a]	-	np[a]	-	np[a]	-	np[a]	-
DVE/**HM**$^+$	np[a]	-	np[a]	-	np[a]	-	np[a]	-

[a] np = no polymerization.

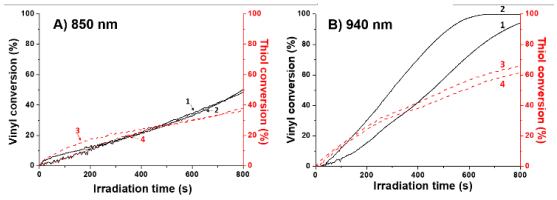

Figure 7. Kinetic profiles of the vinyl and thiol functions of the blend mixture DVE/TT (50/50 wt%) with the NIR **HM**$^+$/Iod system under LED irradiation at A) 850 nm and B) 940 nm in laminate (curves 1 and 3) or under air (curves 2 and 4). Curves 1 and 2: vinyl conversions; curves 3 and 4: thiol conversions. Intensity of light = 1 W.cm^{-2}. [Iod] = 3.8 x 10^{-2} mmol.g^{-1} and [**HM**$^+$] = 6 x 10^{-3} mmol.g^{-1}.

Interestingly, the vinyl and thiol conversions under air in the DVE/TT/**HM**$^+$/Iod formulation are similar to the ones observed in laminate. The EPR spin trapping experiments are consistent with the formation of thiyl radicals when **HM**$^+$/Iod/TT is irradiated as the contribution of •DMPO-SR adduct strongly increases beyond that arising from the Forrester-Hepburn mechanism in the control without light.[54] Figure 8 shows the normalized experimental EPR spectra measured upon photoexcitation of **HM**$^+$/Iod/TT/DMPO under argon along with their simulations, evidencing the presence of superimposed spectral components attributed to the individual DMPO-adducts, with: i) the dominant signal (88%) of •DMPO-SR adduct characterized by the spin-Hamiltonian parameters a_N = 1.364 mT, a_H = 1.276 mT, a_H^β = 0.086 mT, a_H^γ = 0.105 mT; g = 2.0061, ii) the less-abundant signals of the DMPO-methylphenyl adduct (a_N = 1.425 mT, a_H = 2.083 mT; g = 2.0060, 4%), and iii) a carbon-centered radical on **HM**$^+$ (g= 2.0027, 8%). In fact, an electron transfer reaction occurs between **HM**$^+$ and Iod, affording a methylphenyl radical Ar$^\bullet$ (Scheme 2). The latter abstracts a hydrogen atom from TT, thus generating a thiyl radical (R-S$^\bullet$). In laminate, thiyl radicals react with the vinyl group of DVE according to a thiol-ene reaction process. In contrast, oxygen is consumed and reacts with thiyl radicals to form peroxy radicals (RSOO$^\bullet$) under air. The latter can subsequently abstract a hydrogen atom from the thiol functional group of TT to regenerate again thiyl radicals which are highly reactive towards vinyl groups of DVE. These results perfectly fit other UV-visible-sensitized thiol-ene systems previously described in literature.[55,56] Even if vinyl ether derived monomers are prompt to cationic polymerization with photoacids, the absence of cationic photopolymerization of the photosensitive DVE/**HM**$^+$/Iod formulation (Table 2) reinforces the thiol-ene reaction process of the NIR-photosensitized DVE/TT/**HM**$^+$/Iod system. We also underline that the high NIR absorption of **HM**$^+$ at 940 nm can explain the 100% vinyl conversion of DVE under LED@940 nm irradiation compared to the slower conversion under LED@850 nm.

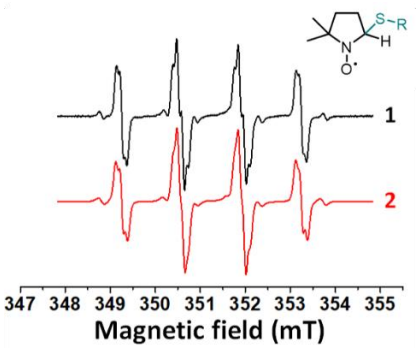

Figure 8. Experimental (1) and simulated (2) EPR spectra obtained during 210 s after exposure (LED@850 nm) of **HM**$^+$/Iod/TT/DMPO in CH_2Cl_2 under argon (initial concentrations: [**HM**$^+$] = 30 mM; [Iod] = 30 mM; [TT] = 375 mM; [DMPO] = 0.08 M). EPR spectrometer settings: microwave frequency, ~9.86 GHz; microwave power, 10 mW; center field, ~350 mT; sweep width, 7 mT; gain, 60 dB; modulation amplitude, 0.05 mT; sweep time, ~42 s; time constant, 10.24 ms; and number of scans, 5. The inset shows the structure of the DMPO-adduct assigned from the simulated EPR spectrum.

Conclusions

The use of NIR-emitting LEDs and a specifically designed NIR-absorbing cyanine opened new opportunities in the radical and thiol-ene photopolymerizations. An unprecedented polymethine derivative incorporating three benzo[*cd*]indole heterocycles was synthesized and evaluated as an efficient photosensitizer of a iodonium salt for NIR-photosensitized polymerization. At the cornerstone of this study, EPR spin trapping experiments revealed the formation of radical initiating species. The addition of a reducing agent (MDEA) to the **HM**$^+$/Iod photoinitiating system clearly highlighted a reversible mechanism leading to the regeneration of **HM**$^+$ and the increase of the acrylate final conversions under LEDs@850 and 940 nm. Additionally, and for the first time, the formation of radical initiating species (*e.g.*, aminoalkyl radicals) was observed by EPR spin trapping experiments under NIR irradiation of the **HM**$^+$/Iod/MDEA system. Remarkably, the suggested **HM**$^+$/Iod/TT formulation successfully promoted the thiol-reaction process on a vinyl ether derivative monomer leading to the 100% consumption of the vinyl functional groups in air or in oxygen-free conditions, especially with LED@940 nm excitation. This work might pave the way to the design of novel encapsulated cells/biological tissues-based hydrogels using NIR light compatible with the biological transparency

window, thus limiting the risks of cells/biological tissues degradation.

Acknowledgements

This work was partly supported by the *Agence Nationale de la Recherche*, in the frame of the SOCOOL project (ANR-20-CE07-0024). This work used the computational resources of the CCIPL/GliCiD computational center installed in Nantes. DLV would like to thank UPEC and CNRS for financial support.

References

[1] J. Zhang, P. Xiao, *Polym. Chem.* **2018**, *9*, 1530–1540.

[2] L. Pierau, C. Elian, J. Akimoto, Y. Ito, S. Caillol, D.-L. Versace, *Prog. Polym. Sci.* **2022**, *127*, 101517.

[3] C. Schmitz, Y. Pang, A. Gülz, M. Gläser, J. Horst, M. Jäger, B. Strehmel, *Angew. Chem. Int. Ed.* **2019**, *58*, 4400–4404.

[4] B. Strehmel, C. Schmitz, K. Cremanns, J. Göttert, *Chem. – Eur. J.* **2019**, *25*, 12855–12864.

[5] B. Strehmel, C. Schmitz, C. Kütahya, Y. Pang, A. Drewitz, H. Mustroph, *Beilstein J. Org. Chem.* **2020**, *16*, 415–444.

[6] Y. Pang, S. Fan, Q. Wang, D. Oprych, A. Feilen, K. Reiner, D. Keil, Y. L. Slominsky, S. Popov, Y. Zou, B. Strehmel, *Angew. Chem. Int. Ed.* **2020**, *59*, 11440–11447.

[7] S. Daehne, U. Resch-Genger, O. S. Wolfbeis, Eds. , *Near-Infrared Dyes for High Technology Applications*, Springer Netherlands, Dordrecht, **1998**.

[8] M. Matsuoka, Ed. , *Infrared Absorbing Dyes*, Springer US, Boston, MA, **1990**.

[9] J. Fabian, H. Nakazumi, M. Matsuoka, *Chem. Rev.* **1992**, *92*, 1197–1226.

[10] G. Qian, Z. Y. Wang, *Chem. – Asian J.* **2010**, *5*, 1006–1029.

[11] Kenry, Y. Duan, B. Liu, *Adv. Mater.* **2018**, 1802394.

[12] H. Zhu, P. Cheng, P. Chen, K. Pu, *Biomater. Sci.* **2018**, *6*, 746–765.

[13] P. Brogdon, H. Cheema, J. H. Delcamp, *ChemSusChem* **2018**, *11*, 86–103.

[14] S. Pascal, S. David, C. Andraud, O. Maury, *Chem. Soc. Rev.* **2021**, *50*, 6613–6658.

[15] E. Hemmer, A. Benayas, F. Légaré, F. Vetrone, *Nanoscale Horiz.* **2016**, *1*, 168–184.

[16] M. Uo, E. Kudo, A. Okada, K. Soga, Y. Jogo, *J. Photopolym. Sci. Technol.* **2009**, *22*, 551–554.

[17] P. Xiao, J. Zhang, F. Dumur, M. A. Tehfe, F. Morlet-Savary, B. Graff, D. Gigmes, J. P. Fouassier, J. Lalevée, *Prog. Polym. Sci.* **2015**, *41*, 32–66.

[18] J. Yeow, S. Shanmugam, N. Corrigan, R. P. Kuchel, J. Xu, C. Boyer, *Macromolecules* **2016**, *49*, 7277–7285.

[19] J. Xu, S. Shanmugam, C. Fu, K.-F. Aguey-Zinsou, C. Boyer, *J. Am. Chem. Soc.* **2016**, *138*, 3094–3106.

[20] S. Shanmugam, J. Xu, C. Boyer, *Angew. Chem. Int. Ed.* **2016**, *55*, 1036–1040.

[21] T. G. McKenzie, Q. Fu, M. Uchiyama, K. Satoh, J. Xu, C. Boyer, M. Kamigaito, G. G. Qiao, *Adv. Sci.* **2016**, *3*, 1500394.

[22] S. Shanmugam, J. Xu, C. Boyer, *Polym. Chem.* **2016**, *7*, 6437–6449.

[23] H. Mokbel, B. Graff, F. Dumur, J. Lalevée, *Macromol. Rapid Commun.* **2020**, *41*, 2000289.

[24] A. Bonardi, F. Bonardi, G. Noirbent, F. Dumur, C. Dietlin, D. Gigmes, J.-P. Fouassier, J. Lalevée, *Polym. Chem.* **2019**, *10*, 6505–6514.

[25] J. L. Bricks, A. D. Kachkovskii, Y. L. Slominskii, A. O. Gerasov, S. V. Popov, *Dyes Pigments* **2015**, *121*, 238–255.

[26] M. Panigrahi, S. Dash, S. Patel, B. K. Mishra, *Tetrahedron* **2012**, *68*, 781–805.

[27] W. Sun, S. Guo, C. Hu, J. Fan, X. Peng, *Chem. Rev.* **2016**, *116*, 7768–7817.

[28] D. Saccone, S. Galliano, N. Barbero, P. Quagliotto, G. Viscardi, C. Barolo, *Eur J Org Chem* **2016**, *2016*, 2244–2259.

[29] K. J. Thorley, J. M. Hales, H. Kim, S. Ohira, J.-L. Brédas, J. W. Perry, H. L. Anderson, *Chem. – Eur. J.* **2013**, *19*, 10370–10377.

[30] B. Li, S. Zhang, L. Tang, Q. Zhou, *Polym. J.* **2001**, *33*, 263–269.

[31] S. Pascal, A. Haefele, C. Monnereau, A. Charaf-Eddin, D. Jacquemin, B. Le Guennic, C. Andraud, O. Maury, *J. Phys. Chem. A* **2014**, *118*, 4038–4047.

[32] S. S. Matikonda, G. Hammersley, N. Kumari, L. Grabenhorst, V. Glembockyte, P. Tinnefeld, J. Ivanic, M. Levitus, M. J. Schnermann, *J. Org. Chem.* **2020**, *85*, 5907–5915.

[33] R. M. Exner, F. Cortezon-Tamarit, S. I. Pascu, *Angew. Chem. Int. Ed.* **2021**, *60*, 6230–6241.

[34] T. Brömme, D. Oprych, J. Horst, P. S. Pinto, B. Strehmel, *RSC Adv.* **2015**, *5*, 69915–69924.

[35] B. Strehmel, C. Schmitz, T. Bromme, A. Halbhuber, D. Oprych, J. S. Gutmann, *J. Photopolym. Sci. Technol.* **2016**, *29*, 111–121.

[36] A. Shiraishi, Y. Ueda, M. Schlapfer, C. Schmitz, T. Bromme, D. Oprych, B. Strehmel, *J. Photopolym. Sci. Technol.* **2016**, *29*, 609–615.

[37] A. Shiraishi, H. Kimura, D. Oprych, C. Schmitz, B. Strehmel, *J. Photopolym. Sci. Technol.* **2017**, *30*, 633–638.

[38] C. Schmitz, A. Halbhuber, D. Keil, B. Strehmel, *Prog. Org. Coat.* **2016**, *100*, 32–46.

[39] C. Kütahya, C. Schmitz, V. Strehmel, Y. Yagci, B. Strehmel, *Angew. Chem. Int. Ed.* **2018**, *57*, 7898–7902.

[40] Y. Pang, A. Shiraishi, D. Keil, S. Popov, V. Strehmel, H. Jiao, J. S. Gutmann, Y. Zou, B. Strehmel, *Angew. Chem. Int. Ed.* **2021**, *60*, 1465–1473.

[41] A. Kocaarslan, C. Kütahya, D. Keil, Y. Yagci, B. Strehmel, *ChemPhotoChem* **2019**, *3*, 1127–1132.

[42] L. Strekowski, J. C. Mason, M. Say, H. Lee, R. Gupta, M. Hojjat, *Heterocycl. Commun.* **2005**, *11*, 129–134.

[43] B. Li, L. Lu, M. Zhao, Z. Lei, F. Zhang, *Angew. Chem. Int. Ed.* **2018**, *57*, 7483–7487.

[44] H. Mokbel, G. Noirbent, D. Gigmes, F. Dumur, J. Lalevée, *Beilstein J. Org. Chem.* **2021**, *17*, 2067–2076.

[45] C. Reichardt, *Chem. Rev.* **1994**, *94*, 2319–2358.

[46] S. S. Matikonda, D. A. Helmerich, M. Meub, G. Beliu, P. Kollmannsberger, A. Greer, M. Sauer, M. J. Schnermann, *ACS Cent. Sci.* **2021**, *7*, 1144–1155.

[47] I. Davydenko, S. Barlow, R. Sharma, S. Benis, J. Simon, T. G. Allen, M. W. Cooper, V. Khrustalev, E. V. Jucov, R. Castañeda, C. Ordonez, Z. Li, S.-H. Chi, S.-H. Jang, T. C. Parker, T. V. Timofeeva, J. W. Perry, A. K. Y. Jen, D. J. Hagan, E. W. Van Stryland, S. R. Marder, *J. Am. Chem. Soc.* **2016**, *138*, 10112–10115.

[48] H. C. Friedman, E. D. Cosco, T. L. Atallah, S. Jia, E. M. Sletten, J. R. Caram, *Chem* **2021**, *7*, 3359–3376.

[49] B. Le Guennic, D. Jacquemin, *Acc. Chem. Res.* **2015**, *48*, 530–537.

[50] F. Peyrot, S. Lajnef, D.-L. Versace, *Catalysts* **2022**, *12*, 772.

[51] C.-W. Hsu, H. Sundén, *Org. Lett.* **2018**, *20*, 2051–2054.

[52] P. Sautrot-Ba, J.-P. Malval, M. Weiss-Maurin, J. Paul, A. Blacha-Grzechnik, S. Tomane, P.-E. Mazeran, J. Lalevée, V. Langlois, D.-L. Versace, *ACS Sustain. Chem. Eng.* **2018**, *6*, 104–109.

[53] Q. Wang, S. Popov, A. Feilen, V. Strehmel, B. Strehmel, *Angew. Chem. Int. Ed.* **2021**, *60*, 26855–26865.

[54] D. I. Potapenko, E. G. Bagryanskaya, Y. P. Tsentalovich, V. A. Reznikov, T. L. Clanton, V. V. Khramtsov, *J. Phys. Chem. B* **2004**, *108*, 9315–9324.

[55] C. Lorenzini, A. Haider, I.-K. Kang, M. Sangermano, S. Abbad-Andalloussi, P.-E. Mazeran, J. Lalevée, E. Renard, V. Langlois, D.-L. Versace, *Biomacromolecules* **2015**, *16*, 683–694.

[56] C. E. Hoyle, C. N. Bowman, *Angew. Chem. Int. Ed.* **2010**, *49*, 1540–1573.